Molecular Dynamics Simulations of Neutral Chlorpromazine in Zwitterionic Phospholipid Monolayers

Mónica Pickholz,[†] Osvaldo N. Oliveira, Jr.,[‡] and Munir S. Skaf*[,†]

Instituto de Química, Universidade Estadual de Campinas-UNICAMP, C.P. 6154, Campinas, SP 13083-970, Brazil, and Instituto de Física de São Carlos, Universidade de São Paulo, C.P. 780, São Carlos, SP 13560-970, Brazil

Received: November 18, 2005; In Final Form: March 8, 2006

Molecular dynamics simulations have been performed to investigate the interactions between chlorpromazine (CPZ), a neuroleptic drug used in the treatment of psychiatric disorders, and dipalmitoylphosphatidylcholine (DPPC), a zwitterionic phospholipid, in Langmuir monolayers. The results from simulations carried out at different monolayer surface densities were able to capture important features of the CPZ−lipid interaction. We find that neutral (unprotonated) CPZ is preferentially located in the lipid tail region of the phospholipids, in little contact with the aqueous phase, and that the orientation of its rigid ring structure and tail conformation vary with lipid surface density. CPZ is found to promote ordering of the lipid tails for all surface densities because of a reduction in the effective surface area per lipid upon addition of the drug. Similar effects have been observed in previous studies of cholesterol in DPPC monolayers, in which lipid tails were seen to order around the solute. This feature, however, is quite distinct from what we observe for the most dense monolayer considered here (area per lipid of 50 Å^2), for which we find that CPZ promotes a local distortion of the lipid tails in its immediate vicinity and a concomitant ordering of lipid tails located further away from the solute. This view is further supported by the results obtained for an approximated nonlinear vibrational sum frequency generation susceptibility, which showed greater tail disorder close to CPZ.

I. Introduction

The interaction of drugs and peptides with phospholipid monolayers and bilayers has long been investigated because of the obvious biological implications, as these phospholipid systems serve as simple membrane models.[1,2] The aim of such studies includes the determination of the guest molecule location, dependence on its concentration, and, ultimately, identification of the overall effects on the model membrane properties. In this context, Langmuir monolayers have been widely employed as they allow one to probe the effects at different surface coverages. Regarding the possible correlation with the biological activity of the guest molecules, recent experimental results have demonstrated that very small amounts of drug or peptide may cause measurable changes in the monolayer properties.[3,4]

Chlorpromazine (CPZ) is a neuroleptic drug of the phenothiazine group widely used in the treatment of psychiatric disorders. Many phenothiazine derivatives, such as CPZ and TFP (trifluoperazine), show high affinity for biomembranes because of their amphiphilic nature.[5] These molecules can easily penetrate the central nervous system[6] and are among the most potent antipsychotic agents.[7] Interactions of CPZ and TFP with biological membranes are associated with various effects in cellular systems, including a protective effect on red cell osmolysis.[8] Experiments on model membranes and monolayers have provided molecular-level evidence that CPZ interacts with the membrane phospholipids, especially the negatively charged ones, and perturbs the membrane structure.[4,9] The partition coefficient of CPZ into the lipid membrane decreases with the increasing phospholipid alkyl chain length, and can be additionally reduced by the presence of cholesterol.[10,11]

Despite the efforts devoted to the study of the interactions of phenothiazines with biomembranes[12−18] and their effects upon the structure of phospholipid monolayers,[3,4] very little is known about the behavior of membranes in the presence of these drugs on a detailed molecular level. Given the therapeutic value of CPZ to human health and the unique capabilities of molecular dynamics (MD) simulations to unravel solvation properties of molecules in lipid bilayers and monolayers,[19−23] it is interesting to perform MD simulations on CPZ−monolayer systems.

In this work, we investigate how CPZ affects DPPC (dipalmitoylphosphatidylcholine) monolayers in the lamellar phase by means of MD simulations of neat and CPZ-containing DPPC monolayers of different surface coverage. The main goal of this work is to provide a molecular-level description of the structural features of CPZ−DPPC monolayers, including the relative location and orientation of the drug with respect to the monolayer and the impact of CPZ upon the ordering of the model membrane. We have considered systems of surface area ranging from 50 to 80 Å^2 per lipid, which are expected to describe DPPC monolayers spanning from an ordered liquid condensed phase, at low surface area (50 Å^2/lipid), to a more disordered fluidlike liquid expanded phase at high area per lipid (80 Å^2/lipid).[24,25] Under similar thermodynamic conditions, previous computer simulations on DPPC monolayers have found a phase transition around 60−65 Å^2/lipid associated with lipid tail order−disorder.[26] It is known that the more ordered phase is characterized by the alignment of lipid chains, predominantly in trans conformation, roughly parallel to the interface normal, whereas in the disordered phase the tails are no longer aligned

* Address correspondence to this author. E-mail: skaf@iqm.unicamp.br. Fax: 55 19 3788 3023.
[†] Universidade Estadual de Campinas-UNICAMP.
[‡] Universidade de São Paulo.

10.1021/jp056678o CCC: $33.50
Published on Web 04/08/2006

and the presence of gauche conformation is substantial. Although no detailed investigation on the phase boundary and phase transition is presented here, our results are consistent with this description and we find that, overall, CPZ tends to promote ordering of the lipid tails. The mechanism by which this ordering is promoted differs as one goes from an essentially disordered, lower surface density system to the liquid condensed phase at 50 Å^2/lipid.

Specification of the charge or ionization state of the solute is an important issue that cannot be overlooked in simulating these systems. Both CPZ and TFP molecules have an ionizable amino group with p*K* values of 8.6 and 8.1,[27] respectively, in pure aqueous solutions, so that both charged (protonated) and uncharged species are likely present in solutions at physiological pH, with predominance of the former. Some studies performed on lipid membranes have indicated that, at physiological pH values of the aqueous phase, CPZ may remain protonated,[12] which causes it to be located preferably in the membrane−water interface.[13−15] Its binding sites, including the carboxylate groups, appear to be located near the membrane surface according to electron spin resonance (ESR) studies.[16] Other experimental results provide evidence that CPZ may also penetrate into the acyl chain region of phospholipid membranes, affecting the acyl chain order[17] and lipid phase transition,[13,18] which is suggestive of a noncharged state of the solute. At pH 9.0, CPZ appears to be mainly unprotonated and neutral.[12] Its location relative to the interface at such high pH values of the solution is difficult to determine because of the large scattering effects that render the absorption measurements unreliable.[28]

It has long been known, however, that the p*K* value of dyes and other organic molecules is sensitive to the local environment at the surface of micelles, biomembranes, monolayers, and other interfaces. Significant p*K* shifts can be induced by the interfacial ambient relative to pure aqueous solutions under similar thermodynamic and pH conditions.[29] The p*K* shifts depend on the membrane type and can be modulated in terms of the partition coefficient ratio of both nonionized and ionized forms of the solute and the surface charge density at the lipid/water interface.[30] For the phenothiazine derivative TFP, more specifically, it has been shown that the ionization constant is downshifted from 8.1 to 7.6 in the presence of egg PC (phosphatidylcholine) multilamellar vesicles.[31] Because of the similarity between the two phenothiazines, similar behavior is expected for CPZ in neutral membranes, that is, an increased neutral-to-protonated ratio relative to that in pure aqueous solutions. Therefore, simulations with neutral and protonated forms of CPZ should be independently carried out to elucidate how both charged and uncharged CPZ species interact with model membranes and, hence, establish a closer correspondence with experiments. As part of a more complete study, in this work we focus our attention on uncharged CPZ only. A comparative study involving charged and neutral CPZ in zwitterionic and anionic phospholipid monolayers will be presented elsewhere.[32]

In the next section, we describe the systems studied and the computational details. In Section III we look at the behavior of CPZ solvated into the lipid monolayers as a function of surface coverage. In Section IV we investigate the main effects of CPZ upon the monolayers, focusing on the overall organization of the different components of the system and how the lipid headgroups and tails are perturbed by the presence of the drug. Our concluding remarks are presented in Section V.

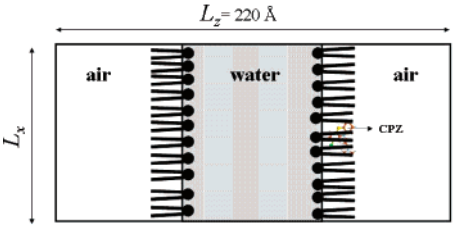

Figure 1. Scheme of the simulation unit cell.

II. Methods and Computational Details

The simulated systems consist of a periodically replicated cell containing 72 lipids, divided into two monolayers with 36 lipids each and a single CPZ molecule. The monolayers are separated by a slab containing 4188 water molecules, as depicted in Figure 1. The simulation geometry is similar to that proposed by Feller and co-workers[33] and has been used in many recent studies.[34−36] Although computationally more expensive than the effective monolayer geometry employed by Kaznessis et al.,[26] the present simulation box permits the study of CPZ-containing and CPZ-free monolayers simultaneously, thus facilitating comparison. Because of the significant molecular volume of CPZ, the surface densities on each monolayer may differ in this approach. An accurate account of such effects could be obtained from a calculation of the pressure profile[37] or through a constant surface tension simulation.[38] These calculations, however, require much longer simulation times and bigger systems than the ones used here. It is also not clear what would be the effect of CPZ on the monolayer density. Different foreign molecules lead to distinct changes in the area per lipid. Halothane, for instance, increases the area per lipid in DPPC bilayers, while the similar solute hexafluroethane yields the opposite behavior.[39]

The system is effectively periodic in 3D and very little (or null) interaction is expected in the *z* direction (normal to the interfaces) because of the large air region. The NAMD2 program[40] was used for the simulations with the PARAM27 CHARMM parameter set.[41] The water molecules were described by the TIP3P model.[42] Intramolecular parameters for neutral CPZ were obtained from quantum chemical calculations, as described below. The intermolecular Lennard-Jones parameters were obtained by analogy with similar molecules already parametrized within the CHARMM approach. The 2-monolayer systems were constructed from a preequilibrated DPPC bilayer[43] by separating each leaflet into two monolayers which were further equilibrated. A molecule of CPZ was introduced into one of the monolayers yielding a molar concentration of 0.028 M (1:36), while the other monolayer remained CPZ free, as a reference. This concentration of CPZ is typical of experiments with Langmuir monolayers, although effects can be observed also at lower concentrations. The effects caused by CPZ were investigated for four different lipid surface density monolayers, corresponding to 50, 60, 70, and 80 Å^2 per lipid molecule. Henceforth, we shall refer to these systems as **A-50**, **A-60**, **A-70**, and **A-80**, respectively. The size of the simulation cell was adjusted to accommodate the 36 lipids on each interface, always keeping the sides $L_x = L_y$ and $L_z = 220$ Å for every system considered. The number of water molecules was kept constant. The system's dimensions were carefully chosen to ensure an aqueous layer of at least 20 Å between the headgroups of the two opposing monolayers, therefore ensuring negligible interactions between surfaces.[33]

Classical MD simulations were carried out. The system was equilibrated at a temperature of 323 K. The volume, $V = L_x^2 L_z$,

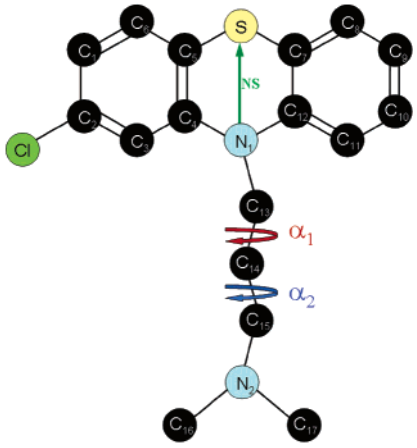

Figure 2. Molecular structure of chlorpromazine and atom numbering. Dihedral angles α1 (N1−C13−C14−C15) and α2 (C13−C14−C15−N2). The vector NS connects nitrogen N1 and sulfur S atoms.

was adjusted to obtain the desired area per lipid, as explained. Following the standard procedures, the simulation of each system consisted of an equilibration period of about 3 ns (NVT ensemble), within which the CPZ molecule migrated to its preferential location relative to the membrane, followed by an unperturbed (NVE) run of 5 ns. A multiple-time step algorithm, RESPA,[44] with the shortest time step of 2 fs was used. During the simulation, all intramolecular motions involving hydrogen atoms were frozen with use of SHAKE/RATTLE algorithms.[45] Short-range forces were computed with a cutoff of 10 Å and long-range forces were taken into account by means of the particle mesh Ewald (PME) technique.[46]

The CPZ molecule was initially placed at the lipid tail−air interface. We have chosen this particular initial configuration after performing several auxiliary tests, which have shown that neutral CPZ ends up at the lipid tail region. A different behavior is found for protonated CPZ, which appears closer to the aqueous phase.[32]

III. Structuring of CPZ Interacting with the DPPC Monolayer

The ground-state geometry of the neutral (unprotonated) chlorpromazine was optimized within the Density Functional Theory (DFT) with use of the B3LYP[47] functional and 6-31G* basis set. The molecular structure of CPZ is shown in Figure 2, along with the atom numbering scheme. The calculated CPZ geometry is in fairly good agreement with the structure determined by X-ray diffraction,[48] with a bent structure in which the side chain of CPZ tilts toward the chlorinated benzene ring. Reports in the literature suggest that this conformation should correlate with biological activity.[49] The partial atomic charges were obtained through a single point HF/6-31G* calculated with ChelpG.[50] No parameters are available in the literature for this molecule and, therefore, we based our parametrization, including intramolecular bond lengths and angles, on the equilibrium geometry just described. The force constants and intermolecular parameters were chosen in analogy to similar molecules already described by CHARMM. Additional information about bonded and nonbonded parameters and partial atomic charges are provided as Supporting Information.

CPZ is a relatively large molecule with little symmetry. The way it binds to the membrane may depend on packing, steric effects, and specific interactions. Entropic effects also may play an important role in the distribution of the drug within the monolayer. To gain insights on the structure of CPZ relative to

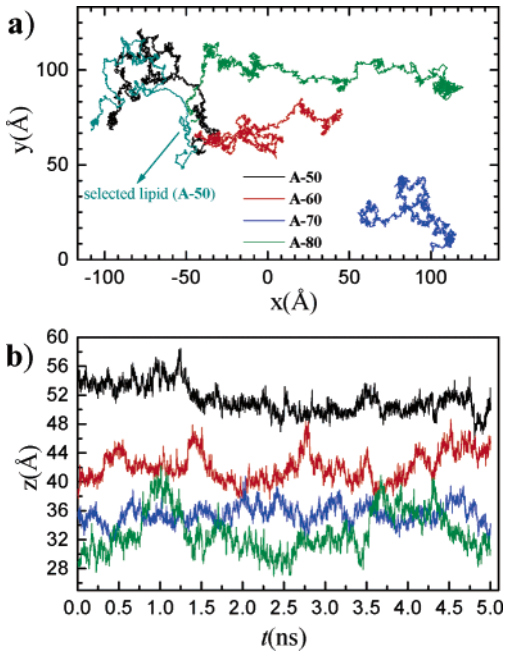

Figure 3. (a) *xy* projection of the center of mass trajectory of CPZ and (b) time evolution of coordinate *z* of CPZ center of mass for the different surface densities: **A-50** (black), **A-60** (red), **A-70** (blue), and **A-80** (green). A selected lipid from the **A-50**/CPZ monolayer is also shown in part a (dark cyan).

the monolayer, we have investigated the displacement of the solute center-of-mass along the interfacial *xy* plane and *z* axis, the orientation distribution of CPZ's rigid ring structure with respect to the interface normal, and the distribution of the distance between the two nitrogen atoms of CPZ in order to investigate its tail conformation (straight-folded). In Figure 3a we show the CPZ center-of-mass NVE trajectory along the *xy* plane and interface normal (*z*) for different surface areas. It can be readily seen that the 5 ns runs were sufficiently long for the molecule to travel across more than one unit cell on the interfacial plane. An additional analysis involving the lipids nearby the solute suggests that the motions of CPZ and lipid molecules in the *xy* plane are correlated, as expected from the large surface area of the rigid ring structure. To illustrate, Figure 3a also depicts the *xy* plane projection of the center-of-mass motion of a selected lipid (dark cyan), indicating that CPZ and lipid molecules wander around the interface on similar time scales. Figure 3b shows the time evolution of the *z* component for each case. The CPZ molecule oscillates in the *z* direction around its average position, with larger standard deviation for **A-80**, the lowest surface density system studied. The solute is never seen to cross from one monolayer to the other. Interestingly, the smallest fluctuations in the *z* component of CPZ center-of-mass are found for system **A-70**.

Because of its rigid structure, it is important to determine whether the CPZ ring has a preferential orientation relative to the interface. This can be done, for instance, by inspecting the orientation of the vector connecting the nitrogen (N_1) and sulfur (S) atoms (see Figure 2, NS vector). Figure 4 shows the results for the probability density, $P(\varphi)$, for NS vector to form an angle φ with the normal to the monolayer, normalized by the isotropic distribution, $P^{iso}(\varphi) = {}^1/_2 \sin \varphi$. Integration of $P(\varphi)/P^{iso}(\varphi)$ over all angles yields unity. The orientation of NS varies with the surface density: For the densest monolayer (**A-50**), this vector makes an angle in the range between 120° and 180°, i.e., pointing essentially toward the lipid tails−air interface. In marked contrast, NS is preferentially oriented at low angles

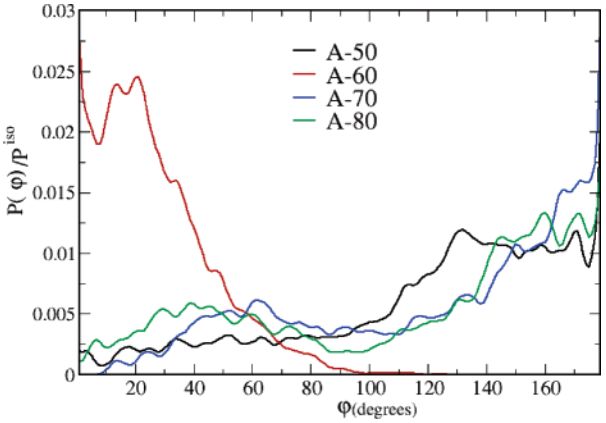

Figure 4. Normalized orientational probability distribution, $P(\varphi)/P^{iso}(\varphi)$, of the φ angle between the NS vector of the CPZ molecule (essentially the orientation of the rigid tricyclic ring) (see Figure 2) and the normal to the monolayer for CPZ at different surface densities.

(<50°) for **A-60**, with vanishingly small probability for angles greater than 90°, which means that NS points preferentially to the lipid head-water interface. For **A-70** and **A-80**, the lowest density cases, NS can be found in a broad distribution of orientations, with larger probability for higher values of φ, indicating orientational disorder of the molecule relative to the monolayer. These features will be rationalized ahead in the light of the charge density profiles.

The distance between nitrogen atoms N_1 and N_2 (Figure 2), ΔN_1N_2, provides an idea of the relative conformation of the CPZ tail. Figure 5 shows ΔN_1N_2 histograms corresponding to each surface density. The distribution can be roughly described as three superimposing Gaussian-like distributions, labeled **A**, **B**, and **C**, corresponding to ΔN_1N_2 average distances of approximately 3.60, 4.65, and 5.05 Å, respectively. These distributions can be associated with three types of molecular geometry according to the trans-gauche conformations of the dihedral angles α1 and α2 (see Figure 2) of the CPZ tail. As illustrated in Figure 5 (top), conformation **A** corresponds to the structure in which both dihedral angles are gauche, **B** corresponds essentially to one trans and another gauche, while conformation **C** occurs when both dihedrals are trans. The population of each of these distributions depends on surface coverage, with conformation **B** being the most frequent for all coverages, except for **A-70**. Conformation **A** becomes important at lower surface densities, especially for **A-70**, for which the more compact conformation of CPZ tail is slightly preferred. It is not unlikely that this feature may underlie the small fluctuations of the *z* coordinate of CPZ center-of-mass for **A-70** discussed above. However, this has not been investigated here. Conformation **C**, in turn, is found to be somewhat insensitive to the surface coverage.

To further illustrate the attributed conformations **A**−**C**, we have depicted in Figure 6 a two-dimensional distribution of angle α_1 versus α_2 for each surface density. For all cases considered, there are four populated regions which correspond essentially to α_1 and α_2 distributed between ∼40° and ∼80° (gauche conformation; **A**) and to α_1 and α_2 spanning from ∼160° to ∼180° (trans conformation; **C**). The central peak **B** arises essentially from two contributions, $\alpha_1-\alpha_2$ trans-gauche and gauche-trans, with the former being somewhat predominant.

In the next sections we investigate how CPZ affects physical properties of the monolayers.

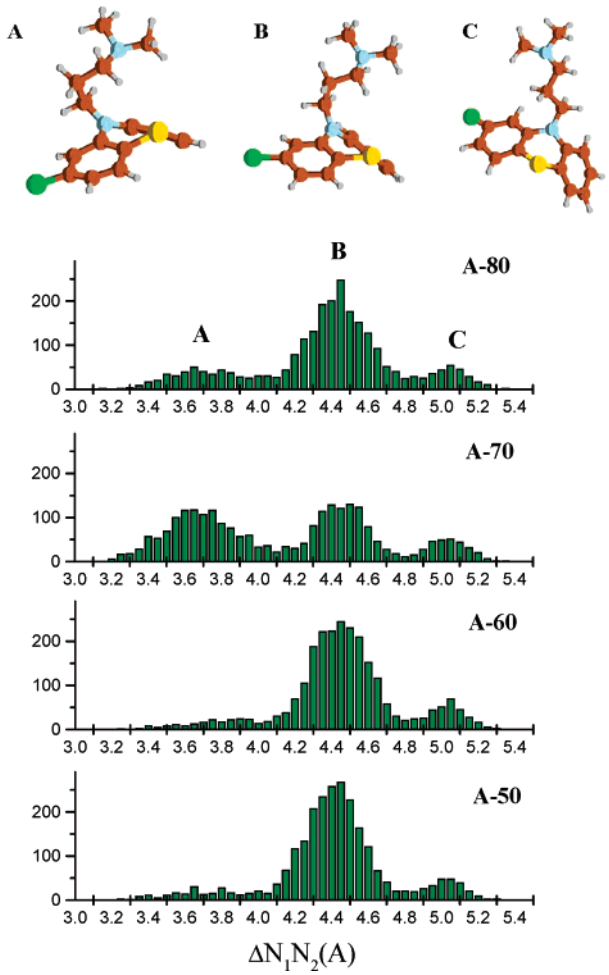

Figure 5. Distribution of the distance between CPZ nitrogens N1 and N2, ΔN1N2, for the simulated monolayers over the 5 ns trajectories. On the top is shown an example of **A** (cis-cis), **B** (cis and trans), and **C** (trans-trans) molecular conformations.

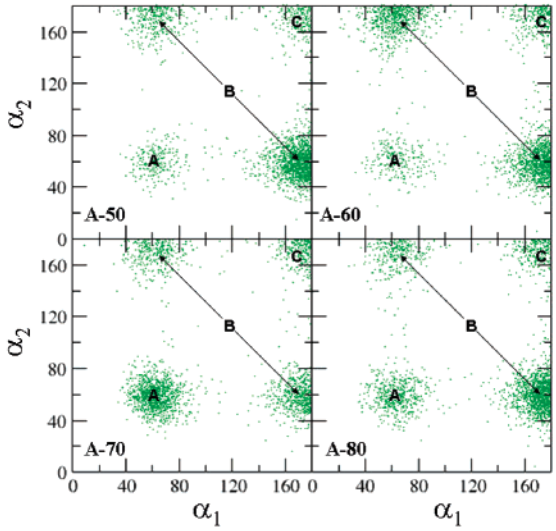

Figure 6. Two-dimensional distributions for the dihedral angles α1 and α2 for the four surface densities considered. Characteristic dihedral angles corresponding conformations **A**−**C** are indicated.

IV. Effects of CPZ on DPPC Monolayers

A. Electron Density Profiles. The interfacial ordering of the system can be evaluated through the electron density profile normal to the monolayer, which has proven useful in describing the structural properties of membranes and may be obtained

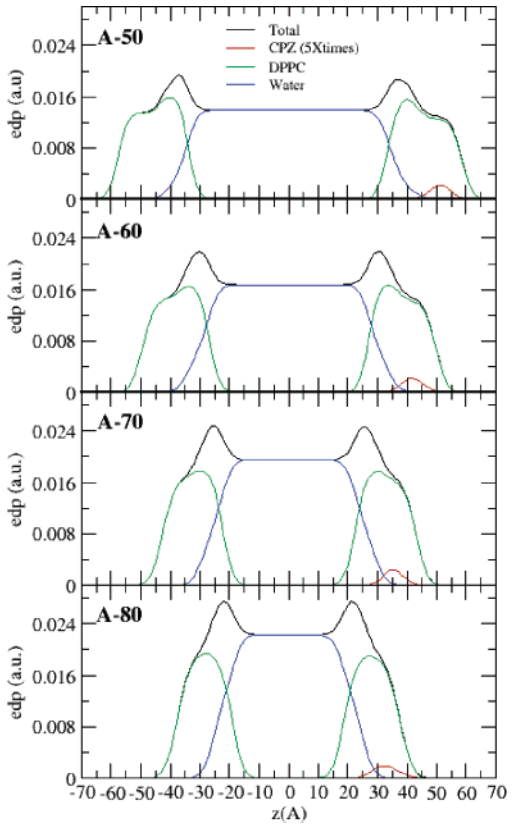

Figure 7. Electron density profile of the different components of the system: water in blue, DPPC monolayers in green, and CPZ in red (5 times amplified for comparison purposes) and the total EDP in black for the different surface coverages **A-50** to **A-80** top to bottom.

from X-ray or neutron scattering experiments.[51] Figure 7 shows the calculated electron density profiles (EDP) for each of the system's constituents (water, DPPC, and CPZ). The profiles were calculated by time averaging the net charge per 0.1 Å thick slabs, assuming a Gaussian distribution centered at the atomic positions and width of approximately 2.0 Å. The contributions from water (blue), CPZ (red; amplified 5 times for comparison purposes), lipids (green), and total (black) EDP are plotted against the z coordinate, where $z = 0$ corresponds to the system center located in the aqueous phase. The EDPs for both monolayers are shown. The left one corresponds to the neat DPPC monolayer, whereas the other contains CPZ. The thickness of the water slab between monolayers increases with increasing surface coverage because the number of water molecules was maintained fixed. We ensured that the water slab had a minimum thickness of 20 Å to prevent effects from the opposing monolayer. Consistent with the literature,[52] as the water electron density decreases to zero, a complex interface emerges where the lipid heads become hydrated. The profiles show that CPZ is solvated mainly within the dry region of the monolayer (right), more specifically in the lipid tail region, superimposing with the upper carbons. CPZ has little access to the water−lipid interface, consistent with the experimental results (at pH ~9.0), in which CPZ is predominantly found at the hydrophobic region of a lipid bilayer.[6,52]

Due to the complexity of the water/lipid interface, it is difficult to estimate its thickness precisely. Here, we estimate the interface thickness using two physically sensible measures. First, we consider the function $f(z)$ defined as the product of the water and lipid electron density profiles. The $f(z)$ function was fitted by a Gaussian and the interface thickness, Δz, is taken as twice the Gaussian half-width. Although somewhat arbitrary,

TABLE 1: Water−Monolayer Interface Thickness, Δz, Number of Water Molecules per Lipid, N_W/N_L, at the Water−Lipid Interface, and Interfacial Width, d, for Each Simulated Surface Density for Neat and CPZ-Containing Monolayers[a]

surface density monolayer	Δz (Å) (neat)	Δz (Å) (CPZ)	N_W/N_L (neat)	N_W/N_L (CPZ)	d (Å) (neat)	d (Å) (CPZ)
A-80	12.4	12.6	19.9	20.3	11.0	11.2
A-70	12.4	12.6	17.4	17.7	11.1	11.2
A-60	13.0	12.4	15.0	14.1	11.1	10.5
A-50	11.0	12.6	9.9	11.1	8.9	10.0

[a] The estimated error for Δz is roughly 0.4 Å for all systems.

this measure turned out quite robust for different monolayers. The estimated values for Δz are shown in Table 1. For neat monolayers, the Δz values for **A-60** to **A-80** are not appreciably different, lying between 12.4 and 13.0 Å. For **A-50**, there is an approximately 10% reduction in thickness to $\Delta z \sim 11.0$ Å, which is associated to the marked decrease in the lipid heads hydration at this surface density, as we shall discuss shortly. This differs somewhat from the results found for neat DPPC monolayers on ionic aqueous solutions, for which the interface thickness increases with surface density.[26] Our results also show that the presence of CPZ has very little effect on interface thickness for systems **A-60** through **A-80**. For these CPZ-containing monolayers Δz remained around 12.6 Å. For **A-50**, however, Δz increases considerably from 11.0 to 12.6 Å in the presence of CPZ, suggesting the appearance of somewhat more prominent interface protusion modes.

Additional quantitative information can be obtained from the shape of the water EDP profile alone. Following Duque et al.,[53] the interfacial width is estimated by fitting the profiles to the function:

$$\mathrm{edp}_{\mathrm{water}}(z) = \frac{\rho_w}{2}\left(1 + \tanh\left(\frac{\alpha(z - z_0)}{d}\right)\right)$$

where ρ_w corresponds to the bulk water EDP value and the constant $\alpha = 2\ \tanh^{-1}\ 0.8 = 2.197$ is chosen so that d corresponds to the 10/90 interfacial thickness. Results for the thickness d (Table 1) are consistent with the Δz estimates, showing that only **A-50** experiences a significant increase in thickness in the presence of CPZ. In Table 1, we also show the average number of water molecules per lipid, N_W/N_L, in the interfacial region, calculated by integrating $\mathrm{edp}_{\mathrm{water}}$ up to the z value corresponding to 95% of ρ_w. We see a decrease in N_W/N_L with increasing surface coverage, for both pure and CPZ-containing monolayers, as one goes from **A-80** to **A-50**. This is consistent with the expected enhancement of the polar head hydration when the area per lipid increases.

Figure 8 shows the EDP for the CPZ molecule separated in terms of the individual group contributions from the tricyclic rigid rings and the tertiary propylamine tail for distinct surface densities. At the lowest surface densities (**A-80** and **A-70**), the distributions are relatively broad (**A-70** being slightly more localized), with ring and tail distribution maxima near each other, suggesting no strong preferential orientation of individual groups (orientational disorder). At these coverages, CPZ is closer to the aqueous phase and its tail points, on the average, slightly away from the lipids (smaller values of z). As the lipid surface density increases (**A-60**), CPZ moves toward the lipid tail region and a clear separation of the group distributions appears in which the CPZ tail points preferentially to the terminal portion of the phospholipid tails and the ring structure points to the lipid headgroups. At **A-50**, however, CPZ moves further into the

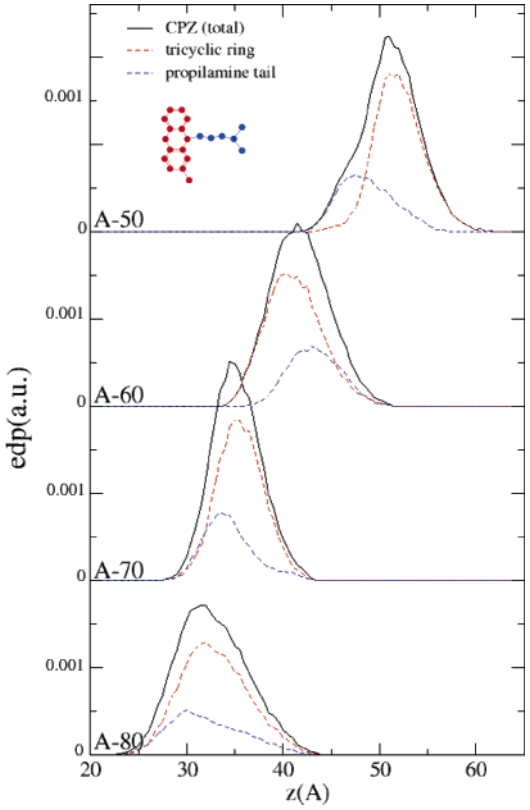

Figure 8. CPZ electron density profile (black) and the partial contribution of the tricyclic ring (red) and propylamine tail (blue) for the different surface densities from **A-50** to **A-80** top to bottom.

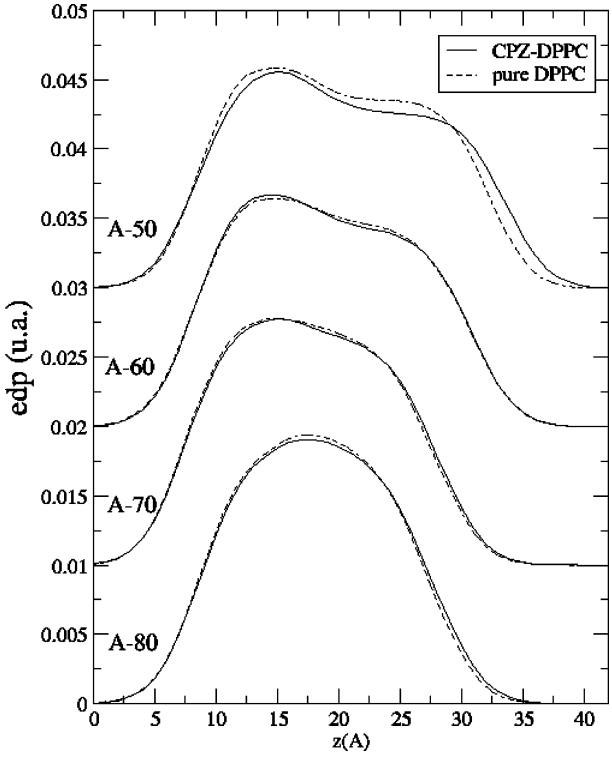

Figure 9. Comparison of the electron density profiles of neat (dashed lines) and CPZ-containing DPPC (solid lines) monolayers for different surface densities.

nonpolar lipid tail region and the tail orientation is now reversed back, pointing preferentially to the lower groups of the lipid heads, while the rigid ring structure is essentially solvated by the lower portions of the phospholipid tails.

These results are consistent with the analysis presented in Section III (cf. Figure 4). Although the orientation of the CPZ tail at **A-70** (or **A-80**) and **A-50** is similar (Figure 4), the underlying reasons seem different: At low surface densities (**A-70** and **A-80**), where CPZ has a relative rotational freedom, the average preferential orientation of the tail is determined by its affinity for the more polar region, whereas at **A-50** the preferential orientation of CPZ appears to be due to packing effects, as the compact structure of the lipid headgroups prevents the bulky part of the solute molecule from entering this region. As we shall see later, at **A-50**, CPZ accommodates within cavities and is located predominantly between the lipid tails. For **A-60**, we believe that an interplay between polarity and packing effects leads to the observed orientation of CPZ. Additional investigation is needed to clarify this feature.

To evaluate how the lipid distribution is affected by surface coverage and presence of CPZ, we show in Figure 9 the calculated EDPs for both CPZ-free and CPZ-containing monolayers, superimposed onto each other by mirror reflection. A change in shape is seen when the area per lipid increases, going from a broad asymmetric distribution for **A-50** (thickness ~40 Å) with a higher density at the water−lipid interface (corresponding to the lipid heads) to a quasi-Gaussian distribution for **A-80** (thickness ~35 Å). This change in shape suggests a phase transition going from **A-50** or **A-60**, as we shall discuss later. The incorporation of the CPZ molecule into the monolayer affects essentially the EDP of the most densely packed case (**A-50**), as the profiles for the lower density surfaces remain practically unaltered. For **A-50**, CPZ broadens the EDP (the whole area under these curves remains constant).

To see whether this effect comes from the lipid headgroups or lipid tails, we take a closer look at the distribution of the different portions of the headgroups in the presence of CPZ. Figure 10 depicts the phospholipid EDP in terms of the choline, phosphate, glycerol, and carbonyl group contributions separately for **A-50**. One finds that CPZ promotes a broader distribution for all groups in the head for **A-50**, consistent with the observed increase of the water−lipid interface thickness. The increase in thickness is roughly 2.5 Å for each group. The broadening of the electron density profiles for **A-50** arises essentially from a prominent increase in the protrusion modes of the lipid monolayer in the presence of CPZ. In marked contrast, the headgroup EDPs for **A-70**, taken as an example of the lower density cases, are practically unaltered by the presence of CPZ.

To understand these features at the molecular level, we take a closer look at the lipid head behavior and the changes caused by CPZ in the next section.

B. Analysis of the Headgroups. The effects from CPZ on the lipid headgroups of the monolayers can be analyzed in more detail by inspecting the orientation probability distribution and the radial distribution function of the charged groups P and N of the zwitterionic lipid heads. Let θ be the angle between the $P^- \rightarrow N^+$ vector and the monolayer normal. The orientation probability distributions, $P(\theta)/P^{iso}(\theta)$, calculated by averaging over all lipids and all configurations (over the 5 ns) are depicted in Figure 11 for each surface density. For an isotropic distribution, $P(\theta)/P^{iso}(\theta)$ is constant. The probability distributions for the neat monolayers (black) are little sensitive to surface density from **A-50** to **A-70**. The preferential orientation is around $\theta \sim 80°$, consistent with the results obtained for a DPPC bilayer.[54] However, for **A-50** the distribution is slightly broader, reflecting an increase in surface roughness. Indeed, larger surface roughness in molecular scale is expected for denser surfaces because of the Coulomb repulsion between lipid heads under compression. For **A-80**, the scenario is more complicated because of

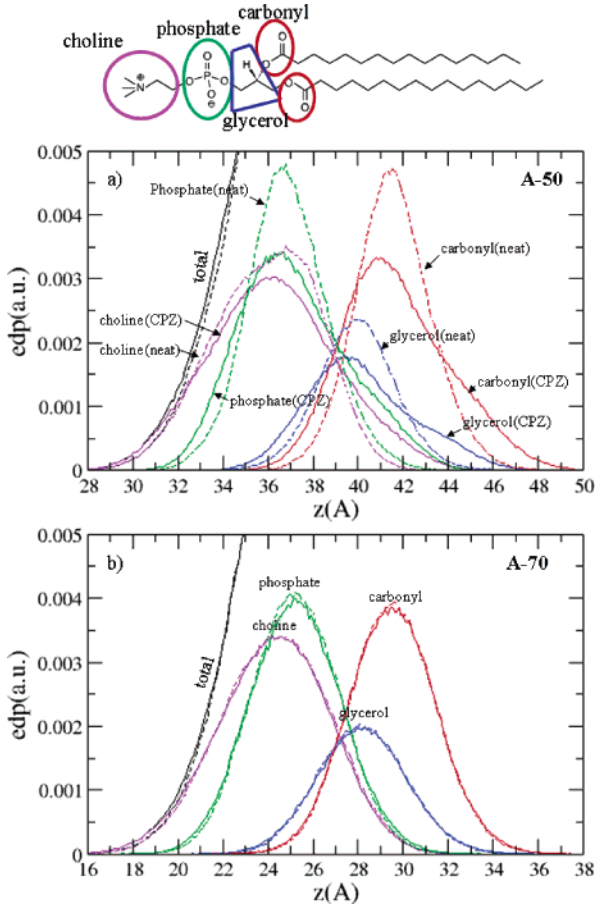

Figure 10. Electron density profiles for the different headgroups, choline (violet), phosphate (green), glycerol (blue), and carbonyl (red), for the neat monolayer (dashed lines), and CPZ/monolayer (solid lines): (a) **A-50** and (b) **A-70**.

the increased disorder that accompanies less dense surfaces. An interplay is likely to exist between the order-promoting lipid interactions and entropy at this surface density. For **A-80**, $P(\theta)/P^{iso}(\theta)$ shows three main structures: a maximum around 60° (also observed for denser surfaces, **A-70** and **A-60**), a main broad feature from 90 to 120°, which indicates that the dipoles are essentially oriented parallel to the *xy* plane, and a small structure near 150°, pointing to the tail region of the monolayer.

In the presence of CPZ, the $P(\theta)/P^{iso}(\theta)$ distributions for the **A-60** and **A-70** cases are slightly affected, with the appearance of a barely perceptible structure around 130°, for instance. For **A-50**, the distribution becomes somewhat more localized and the mean value of θ downshifts to ~50°. For **A-80**, in contrast, $P(\theta)/P^{iso}(\theta)$ becomes much broader in the presence of CPZ. In particular the structures around 90° (PN vector lying flat on the surface) and 130° show a remarkable decrease in the presence of CPZ, leading to a distribution resembling that of higher densities. In this way, CPZ seems to bring an effective increase in surface density.

Further insights into the structure of the headgroups are provided by the radial distribution functions, $g_{\alpha\beta}(r)$. Results are shown in Figure 12 for phosphorus−phosphorus, $g_{PP}(r)$, nitrogen−nitrogen, $g_{NN}(r)$, and phosphorus−nitrogen, $g_{PN}(r)$, distribution functions for neat and CPZ-containing monolayers at **A-50** only (the curves are similar for other surface densities). Overall, our results for the neat surface agree with the literature,[52] confirming the existence of a strong attraction between the choline and the phosphate groups. Although the presence of CPZ introduces very small changes in the radial distribution functions, a

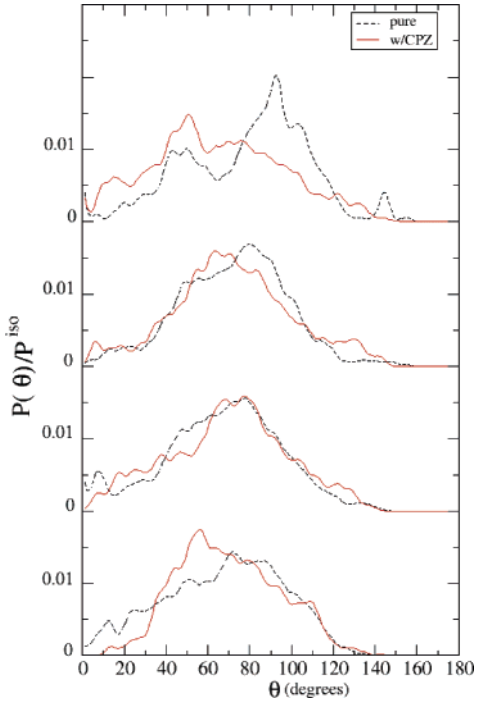

Figure 11. Orientational distribution, $P(\theta)/P^{iso}(\theta)$, of the θ angle between the headgroup PN vector and the bilayer normal for the different surface densities. Neat DPPC are in black and CPZ/DPPC in red.

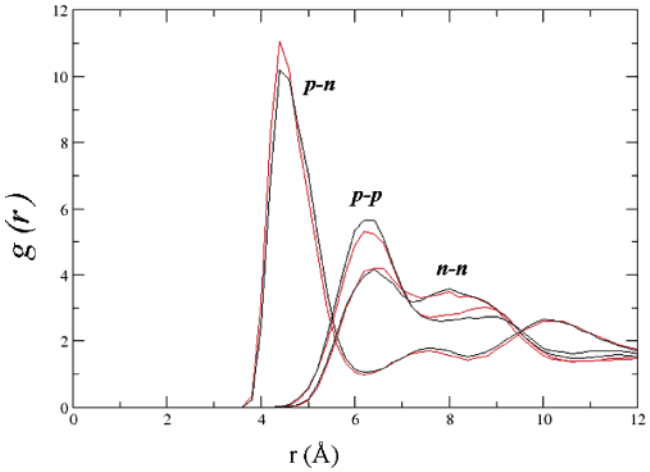

Figure 12. Intermolecular radial distribution functions, $g_{PP}(r)$, $g_{PN}(r)$, and $g_{NN}(r)$. Neat monolayer (black) and CPZ−monolayer (red) for **A-50**.

sharpening in the first peak of $g_{PN}(r)$ can be clearly seen, suggesting that CPZ is responsible for an increase in the lipid headgroup order for the densest case. The intensity of these peaks is strongly affected by the surface density, decreasing when surface density increases. However, the positions of the principal maxima remain unaltered. This can be understood as follows: When the area per lipid increases, more water penetrates into the available free spaces and screens the attractive electrostatic interactions between headgroups, thus enabling an entropy-driven dispersion of lipids in the *z* direction. These features are almost unaffected by the presence of CPZ.

C. Analysis of the Lipid Tails Region. One of the most popular quantities to characterize order in lipid bilayers is the order parameter defined by

$$S_{mol} = \frac{1}{2}\langle 3\cos^2\theta_n - 1\rangle$$

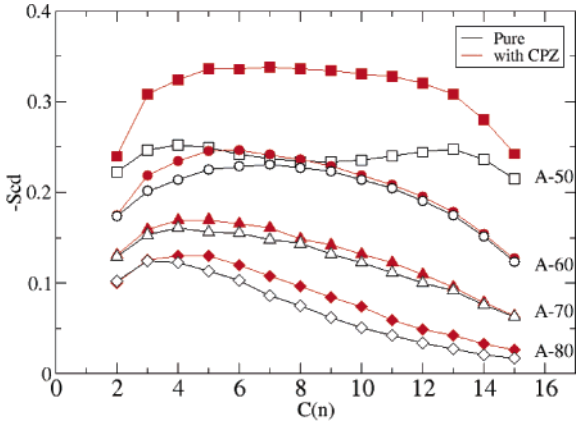

Figure 13. Order parameters ($-S_{CD}$) as a function of the position of the carbon atoms along the hydrocarbon chain of DPPC. Neat DPPC are shown in black and CPZ/DPPC in filled red symbols for the different surface densities: **A-50** (square), **A-60** (circle), **A-70** (triangle), and **A-80** (diamond). The lines are guides to the eyes.

which can be obtained from deuterium NMR measurements. Here, θ_n is the angle between the normal to the bilayer and the normal to the plane defined by two carbon−deuterium (C−D) bonds in a deuterated *n*-methylene group of the lipid acyl chain. $S_{mol} \approx 1$ indicates that the chains are all trans and perpendicular to the bilayer plane, $S_{mol} \approx 0.5$ indicates that they are all trans and parallel to the plane, and $S_{mol} \approx 0$ corresponds to random orientation. The order parameter is related to the tilt angle of the chains and to trans-gauche distribution of chain dihedrals, but the relationship is indirect.

The effects on the lipid packing from guest molecules such as CPZ distributed within membranes can be experimentally determined from changes in the carbon−deuterium segment order parameter along the lipid chain.[54] The experimental order parameter, $S_{CD} = -{}^1/_2 S_{mol}$, is derived from the measured residual quadrupole splitting $\Delta\nu = {}^3/_4(e^2qQ/h)S_{CD}$.[55] It is experimentally challenging to quantify the conformational order in monolayers because NMR and infrared spectroscopy may not be sufficiently sensitive.[56] For DPPC monolayers, Gericke and co-workers[57] suggested that the region near the headgroup is more ordered than the region at the tail end and that compression results in increased ordering of tails (essentially more trans conformations). Experimental results for DPPC bilayers show that the order parameters of the initial segments close to the glycerol and headgroup region display a broad plateau ($|S_{CD}| \sim 0.2$) followed by a reduction in ordering toward the central region of the bilayer.[58] The characteristic order profile is due to the tethering and alignment of the acyl segments near the aqueous interface, with the increased disorder in the bilayer center attributed to chain terminations.

The order parameters of each C−H methylene group have been calculated for every case and the results are shown in Figure 13. The CH_2 groups are numbered consecutively from 2 to 15. The carbonyl and CH_3 carbons are labeled 1 and 16, respectively. The order parameters of pure DPPC monolayers show decreasing order as the area per lipid increases. Consistent with recent studies by Kaznessis et al.[26] and Knecht et al.,[24] a phase transition from a liquid condensed to a liquid disordered phase occurs with increasing areas, which is accompanied by a marked increase in the conformational disorder of the lipid tails. Although there is good agreement in the magnitude of S_{CD}, the shape of S_{CD} curves differs from those reported by Kaznessis et al.[26] for **A-60** and **A-70**. Our results resemble those obtained for lipid bilayers, where a linear decrease was observed at the end of the chain.

One of the main effects of CPZ is that its rigid ring system induces greater order on the hydrocarbon chains, since an increase in S_{CD} was observed for all surface densities upon addition of the drug. For systems **A-60**, **A-70**, and **A-80**, which represent disordered tail phases, the effect is similar to what occurs with cholesterol in DPPC bilayers.[21] For cholesterol, an explanation was given based on the ordering of neighboring DPPC molecules. However, we believe that another mechanism prevails for **A-50**, as we shall discuss shortly. For **A-60**, CPZ seems to affect mostly the ordering of the upper carbons (3 to 8, the most ordered), supported by the hypothesis based on the results from Section IV.A of the CPZ rigid ring structure being preferentially located in the upper part of lipid tails (see Figure 8). Although order parameters for **A-70** are not changed appreciably by addition of CPZ, the drug tends to cause ordering in the carbons from 3 to 13. The more disordered monolayer (**A-80**) is also affected, as the carbons 4 to 15 are ordered in the presence of CPZ.

The effects from CPZ upon tail ordering are considerably more pronounced for **A-50**, the most ordered monolayer (below the transition to a disorder phase). As already mentioned, the **A-50** neat monolayer corresponds to a phase with tail conformational order. The area per lipid for DPPC bilayers in a stable L_α phase is approximately 64 and 62 Å^2/lipid, for experimental[59] and MD simulated[39] bilayers, respectively. This order is further increased in the presence of CPZ, as the results for S_{CD} indicate that more tails adopt the trans conformation parallel to the monolayer normal. A closer inspection of the molecular arrangements reveals that this effect does not stem from a possible ordering of lipid tails in the immediate vicinity of the drug, but rather arises from lipid tails that are located farther apart. Basically, we find that the addition of CPZ into this already ordered phase system creates a local distortion of lipid tails. The local distortion represents an effective compression over the entire monolayer (the area per lipid decreases), which in turn increases order. To illustrate this, we have arbitrarily taken a pair of MD snapshots from the **A-50** monolayer with CPZ, depicted in Figure 14, where a few selected lipids are shown. In Figure 14a, lipids in the immediate neighborhood of CPZ experience a local structural distortion. However, Figure 14b, which depicts lipid molecules located outside the CPZ neighborhood (for clarity, CPZ nearest neighboring lipids are omitted), shows rather clearly that lipids in this region have essentially straight tails in an all-trans conformation, representing a highly ordered liquid condensed state.

In analogy to a two-dimensional liquid−gas (order−disorder) system,[60] we see that above the phase transition, in disordered phases such as **A-70** and **A-80**, the monolayer structure is sufficiently relaxed (compressible) such that CPZ induces order by means of an effective attractive interaction with the lipids. In contrast, for the tail-ordered system **A-50**, CPZ induces additional order by means of an effective compression (repulsive interactions) upon the lipid tails.

Finally, given the recent advances in the use of nonlinear optical spectroscopies to investigate intermolecular structures at interfaces and the positive perspectives for phospholipids monolayers, we have computed an approximated version of the second-order, third-rank tensor, nonlinear susceptibility, $\chi^{(2)}_{ijk}$, obtained from vibrational sum-frequency generation (VSFG) spectral response.[61] According to the recent work by Knecht et al.,[24] a reasonable approximation for the nonlinear susceptibility of phospholipid chains is obtained from[24,62]

$$A_{\chi,CH_i} = N_A\langle\cos\theta_{CH_i}\rangle \qquad (i = 2, 3)$$

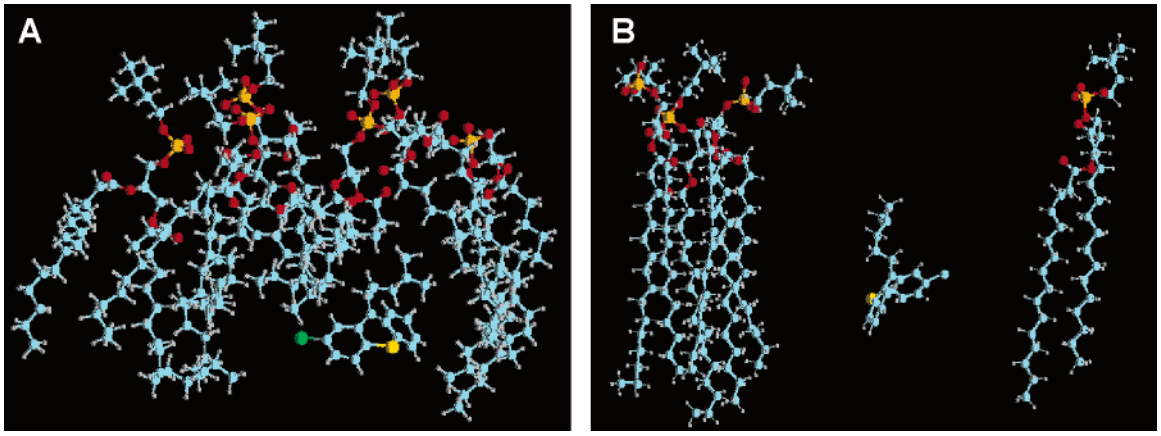

Figure 14. Snapshots of selected configurations from the **A-50** case: (A) neighborhood of CPZ (local distortion) and (B) selected lipids outside the CPZ neighborhood.

where θ_{CH_i} refers to the angle between the direction of the polarization vector and the normal to the monolayer. The polarization vector points along the bisector of the two C−H bond vectors for $i = 2$ and along the terminal C−C bond of the alkyl chain for $i = 3$. N_A denotes the number of lipid molecules per area. Note that this term is also sensitive to the symmetry of the lipid chain conformation: For all-trans conformation the contributions of adjacent methylene groups in the opposite chain have opposite signs and thus cancel on average. Methylene groups yield no net contribution unless the inversion symmetry is broken due to the presence of gauche defects.

In Figure 15 we show the nonlinear susceptibilities A_{χ,CH_3} (a) and A_{χ,CH_2} (b), calculated for both the neat (black) and CPZ-containing (red) DPPC monolayers as functions of surface density. The contributions from CPZ CH_3 and CH_2 groups are negligleable[32] and have been ignored in these calculations. For the highly compressed monolayers (**A-50**) in Figure 15a, the nonlinear susceptibilities A_{χ,CH_3} show high values (strong signal) indicating strong order of the lipid tails. On increasing the area per lipid, the signal decreases rapidly indicating loss of order upon expansion. This behavior was already reported in the literature from both experiments[25] and simulations[24] for neat DPPC monolayers. The effect of CPZ on the monolayer VSFG signal is very subtle: For **A-50** only a very small decrease is observed in A_{χ,CH_3}, suggesting a very slight disorder in the lipid tail caused by CPZ. For small surface density (**A-80**), however, CPZ seems to induce some tail end ordering.

Figure 15b shows stronger A_{χ,CH_2} signal for monolayers of higher surface density, which is also indicative of decreasing order with surface density. Note that the A_{χ,CH_2} signal is about 1 order of magnitude smaller than A_{χ,CH_3} due to cancellations from the alternating contributions mentioned above. The effects from CPZ are more pronounced for the methylene group signal, A_{χ,CH_2}, and also depend on the surface coverage. The A_{χ,CH_2} signal departs further from the perfectly ordered tail value ($A_{\chi,CH_2} = 0$) in going from the neat to the CPZ-containing monolayer for **A-50**, but the reverse is found for less dense surfaces. This behavior, consistent with the trends found for A_{χ,CH_3}, seems to suggest that CPZ brings disorder to a compact monolayer (**A-50**), but order to lower surface density monolayers (**A-70** and **A-80**).

Although the changes in A_{χ,CH_i} due to the presence of CPZ are small, the results above seem, at first glance, to provide a physical picture somewhat different from that portrayed by the S_{CD} order parameters, according to which CPZ induces monolayer ordering for all coverages considered (Figures 13 and 14). To elucidate this apparent discrepancy, we compute the partial

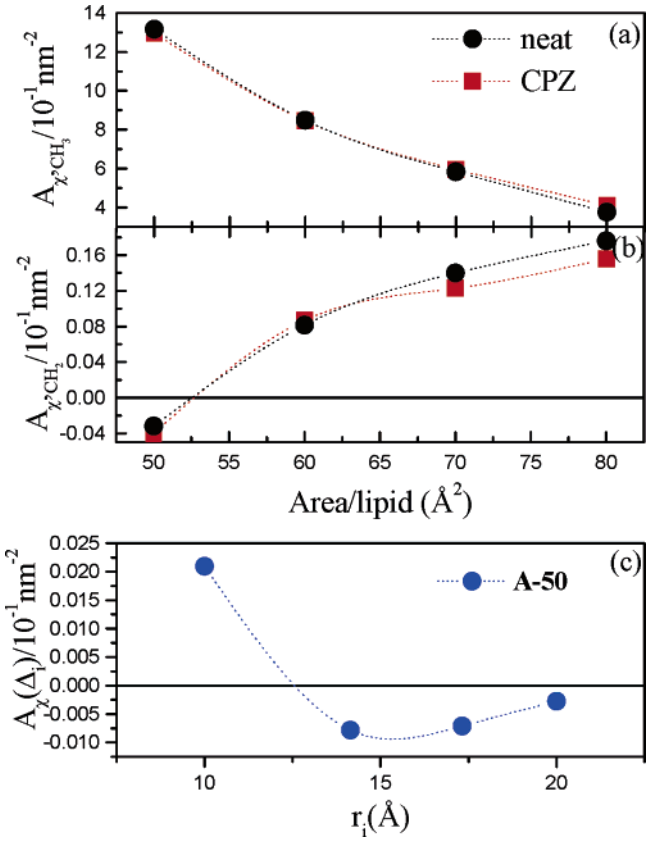

Figure 15. Nonlinear susceptibilities A_χ of the CH_3 (a) and CH_2 (b) groups of both monolayer tails, for neat (black circles) and CPZ-containing monolayers (red squares). (c) Partial CH_2 group contributions to the nonlinear susceptibilities A_χ (Δ_i) from lipids located in concentric cylinders (equal areas, Δ_i) around the CPZ molecule (see text) for the **A-50** monolayer. The lines are guides to the eyes.

methylene group signals, $A_\chi(\Delta_i)$, which are defined for lipid molecules located in different concentric cylindrical shells Δ_i of equal area around the CPZ molecule. Thus, $A_\chi(\Delta_1)$ corresponds to the CH_2 signal from lipids located within the cylinder of radius $r1$ around the CPZ, $A_\chi(\Delta_2)$ corresponds to lipids found in the cylindrical shell defined by $r1 < r < r2$, and so on. Results for $A_\chi(\Delta_i)$ obtained for the compact monolayer **A-50** are depicted in Figure 15c, which shows that the lipid tails in the immediate vicinity of CPZ are considerably more disordered (strong methylene signal) than those located in outer cylindrical shells (signal close to zero). This behavior is fully consistent with the conclusions drawn from the S_{CD} order parameters and

with the local perturbation of the tail structure near the CPZ molecule shown in Figure 14.

V. Summary and Concluding Remarks

We have carried out relatively long MD simulations to investigate the effects from chlorpromazine, an important neuroleptic drug that can partition into the lipid bilayer of cell membranes, on the physical properties of DPPC monolayers as a function of the surface density. Neutral CPZ was preferentially solvated in the tail region of the lipid monolayer with very little access to the water−lipid interface. Water−CPZ contact was shown sensitive to the surface area per lipid, in good agreement with experimental results for CPZ obtained at pH conditions around 9. The orientation of the rigid ring structure of CPZ depended on the surface density: The NS vector pointed preferentially to the lipid tail−air interface for the densest monolayer considered (**A-50**), but was essentially oriented to the aqueous interface for **A-60**. For larger surface areas no preferential orientation of the molecule with respect to the monolayer was found. These findings were corroborated in the analysis of the electron density profiles (EDP). The tail portion of the CPZ molecule may adopt three main conformations associated with the trans-gauche conformations of the dihedral angles formed by CPZ's CH_2 groups with frequencies that were also density dependent on surface coverage. Tail conformation **B**, in which one dihedral is trans and the other gauche, was the most frequent structure for nearly all surface densities, whereas the compact conformation **A**, in which both dihedrals are gauche, was important for **A-70** only. The occurrence of trans-trans conformation **C** was less frequent and practically independent of the lipid surface density.

The analyses of the simulated EDPs showed that CPZ promotes an increase in the water−lipid interface thickness by broadening the distribution profile of the lipid headgroups for the **A-50** monolayer. At lower coverages, however, CPZ had little impact upon the interface EDPs because, in these cases, CPZ could easily be accommodated amidst the lipid molecules. Interestingly, CPZ was found to promote ordering of the lipid tails for all surface densities because of a reduction in the effective surface area per lipid upon addition of the drug. Similar effects have been observed in previous studies of cholesterol in DPPC monolayers, in which lipid tails were seen to order around the solute. This feature, however, was quite distinct from what we observe for the most dense monolayer considered here (**A-50**), for which we find that CPZ promotes a local perturbation of the lipid tails in its immediate vicinity (reducing the methylene groups order parameters) and a concomitant ordering of lipid tails located further away from the solute. This view was further supported by the results obtained for an approximated nonlinear vibrational sum frequency generation susceptibility, which showed greater tail disorder close to CPZ. It would be interesting to see experimental studies of such systems with nonlinear vibrational sum frequency spectroscopy.

Acknowledgment. This work was supported by the Brazilian agencies FAPESP (03/09361-4 to M.S. and 03/07404-8 to M.P.) and CNPq (401913/2003-1 and 479800/2004-9 to M.S.). The authors thank Watson Loh, Eneida de Paula, and Marcel Tabak for discussions and an anonymous reviewer for comments and suggestions.

Supporting Information Available: Additional information about the geometry, topology, and model parameters for CPZ. This material is available free of charge via the Internet at http://pubs.acs.org.

References and Notes

(1) Losche, M.; Sackmann, E.; Mohwald, H. *Ber. Bunsen-Ges. Phys. Chem.* **1983**, *87*, 848.
(2) Weiss, R. M.; McConnell, H. M. *Nature* **1984**, *47*, 310.
(3) Pinto, L. M. A.; Malheiros, S. V. P.; Lino, A. C. S.; de Paula, E.; Perillo, M. A. *Biophys. Chem.* **2006**, *119*, 247.
(4) Hidalgo, A. A.; Caetano, W.; Tabak, M.; Oliveira, O. N., Jr. *Biophys. Chem.* **2004**, *109*, 85.
(5) Chen, J. Y.; Brunauer, L. S.; Chu, F. C.; Helsel, C. M.; Gedde, M. M.; Huesti, W. H. *Biochim. Biophys. Acta* **2003**, *95*, 1616.
(6) Malheiros, S. V. P.; Meirelles, N. C.; de Paula, E. *Biophys. Chem.* **2000**, *89*, 83.
(7) Wisniewska, A.; Wolnicka-Glubisz, A. *Biophys. Chem.* **2004**, *111*, 43.
(8) Brindley, D. N.; Bowley, M. *J. Biochem.* **1975**, *148*, 461.
(9) Chen, S.; Gjerde, A. U.; Holmsen, H.; Nerdal, W. *Biophys. Chem.* **2005**, *117*, 101.
(10) Luxnat, M.; Galla, H. J. *Biochim. Biophys. Acta* **1986**, *856*, 274.
(11) Takegami, S.; Kitamura, K.; Kitade, T.; Hasegawa, K.; Nishihira, A. *J. Colloid Interface Sci.* **1999**, *220*, 81.
(12) Ahyayauch, H.; Goñi, F. M.; Bennouna, M. *J. Liposome Res.* **2003**, *13*, 147.
(13) Nerdal, W.; Gundersen, S. A.; Thorsen, V.; Hoiland, H.; Holmsen, H. *Biochim. Biophys. Acta* **2000**, *1464*, 165.
(14) Agasöler, A. V.; Tungodden, L. M.; Cejka, D.; Bakstad, E.; Sydnes, L. K.; Holmsen, H. *Biochem. Pharmacol.* **2001**, *91*, 37.
(15) Frenzel, J.; Arnold, K.; Nuhn, P. *Biochim. Biophys. Acta* **1978**, *507*, 185.
(16) Louro, S. R. W.; Anteneodo, C.; Wajnberg, E. *Biophys. Chem.* **1998**, *74*, 35.
(17) Römer, J.; Bickel, M. H. *Biochem. Pharmacol.* **1979**, *28*, 799.
(18) Jutila, A.; Söderlund, T.; Pakkanem, A. L.; Huttunen, M.; Kinnunen, P. K. J. *Chem. Phys. Lipids* **2001**, *112*, 151.
(19) Tu, K. C.; Tarek, M.; Klein, M. L.; Scharf, D. *Biophys. J.* **1998**, *75*, 2123.
(20) Koubi, L.; Saiz, L.; Tarek, M.; Scharf, D.; Klein, M. L. *J. Phys. Chem. B* **2003**, *107*, 14500.
(21) Hofsass, C.; Lindahl, E.; Edholm, O. *Biophys. J.* **2003**, *84*, 2192.
(22) Song, Y.; Guallar, V.; Baker, N. A. *Biochemistry* **2005**, *44*, 13425.
(23) Pickholz, M.; Saiz, L.; Klein, M. L. *Biophys. J.* **2005**, *88*, 1524.
(24) Knecht, V.; Müller, M.; Bonn, M.; Marrink, S. J.; Mark, A. E. *J. Chem. Phys.* **2005**, *122*, 024704.
(25) Roke, S.; Schins, J.; Müller, M.; Bonn, M. *Phys. Rev. Lett.* **2003**, *90*, 128101.
(26) Kaznessis, Y. N.; Kim, S.; Larson, R. G. *Biophys. J.* **2002**, *82*, 1731.
(27) Agin, D.; Hersh, L.; Holtzman, D. *Proc. Natl. Acad. Sci. U.S.A.* **1965**, *53*, 952.
(28) Constantinides, P. P.; Inouchi, N.; Tritton, T. R.; Sartorelli, A. C.; Sturtevant, J. M. *J. Biol. Chem.* **1986**, *261*, 10196.
(29) Fernández, M. S.; Fromherz, P. *J. Phys. Chem.* **1977**, *81*, 1755.
(30) Bonnet, P.-A.; Roman, V.; Fatome, M.; Berleur, F. *Chem. Phys. Lipids* **1990**, *55*, 133.
(31) Malheiros, S. V. P.; de Paula, E.; Meirelles, N. C. *Biochim. Biophys. Acta* **1998**, *1373*, 332.
(32) Pickholz, M.; Oliveira, O. N., Jr.; Skaf, M. S. Unpublished.
(33) (a) Feller, S. E.; Zhang, Y.; Pastor, R. W. *J. Chem. Phys.* **1995**, *103*, 10267. (b) Feller, S. E.; Zhang, Y.; Pastor, R. W.; Brooks, R. B. *J. Chem. Phys.* **1995**, *103*, 4613.
(34) Nielsen, S. O.; Lopez, C. F.; Moore, P. B.; Shelley, J. C.; Klein, M. L. *J. Phys. Chem. B* **2003**, *107*, 13911.
(35) Li, Z.; Cranston, B.; Zhao, L.; Choi, P. *J. Phys. Chem. B* **2005**, *109*, 20929.
(36) de Moura, A. F.; Trsic, M. *J. Phys. Chem. B* **2005**, *109*, 4032.
(37) Cantor, R. S. *Biophys. J.* **1999**, *76*, 2625.
(38) Lague, P.; Pastor, R. W.; Brooks, B. R. *J. Phys. Chem. B* **2004**, *108*, 363.
(39) Koubi, L.; Tarek, M.; Bandyopadhyay, S.; Klein, M. L.; Scharf, D. *Anesthesiology* **2002**, *97*, 848.
(40) Kalé, L.; Skeel, R.; Bhandarkar, M.; Brunner, R.; Gursoy, A.; Krawetz, N.; Phillips, J.; Shinozaki, A.; Varadarajan, K.; Schulten, K. *J. Comput. Phys.* **1999**, *151*, 283.
(41) Brooks, B. R.; Bruccoleri, R. E.; Olafson, B. D.; States, D. J.; Swaminathan, S.; Karplus, M. *J. Comput. Chem.* **1983**, *4*, 187.
(42) Jorgensen, W. L.; Chandrasekhar, J.; Madura, J. D. *J. Chem. Phys.* **1983**, *79*, 926.
(43) Structure obtained from Scott Feller's web page: http://persweb.wabash.edu/facstaff/fellers/.

(44) Tuckerman, M. E.; Berne, B. J.; Martyna, G. J. *J. Chem. Phys.* **1992**, *97*, 1990.
(45) Andersen, H. C. *J. Comput. Phys.* **1983**, *52*, 24.
(46) Darden, T.; York, D.; Pedersen, L. J. *J. Chem. Phys.* **1993**, *98*, 10089.
(47) Becke, A. D. *J. Chem. Phys.* **1993**, *98*, 5648.
(48) McDowell, J. J. H. *Acta Crystallogr.* **1969**, *B25*, 2175.
(49) Sakamoto, Y.; Ishii, T.; Kurokawa, N.; Aoki, T.; Ohshoma, S. *J. Mol. Struct.* **1996**, *375*, 259.
(50) Breneman, C. M.; Wiberg, K. B. *J. Comput. Chem.* **1990**, *11*, 361.
(51) Smith, G. S.; Majewski, J. X-ray and Neutron Studies of Lipid Bilayers. In *Lipid Bilayers Structure and Interactions*; Katasaras, J., Gutberlet, T., Eds.; Springer: New York, 2000.
(52) Pasenkiewicz-Gierula, M.; Takaoka, Y.; Miyagawa, H.; Kitamura, K.; Kusumi, A. *Biophys. J.* **1999**, *76*, 1228.
(53) Duque, D.; Pàmies; J. C.; Vega, L. F. *J. Chem. Phys.* **2004**, *121*, 11395.
(54) Tu, K.; Tobias, D.; Blasie, J. K.; Klein, M. L. *Biophys. J.* **1995**, *70*, 595.
(55) Boden, N.; Jones, S. A.; Sixt, F. *Biochemistry* **1991**, *30*, 2146.
(56) Seelig, A.; Seelig, J. *Biochemistry* **1974**, *13*, 4839.
(57) Gericke, A.; Moore, D. J.; Erukulla, R. K.; Bittman, R.; Mendelsohn, R. *J. Mol. Struct.* **1996**, *379*, 227.
(58) See, for instance, Tieleman, D. P.; Berendsen, H. J. C. *J. Chem. Phys.* **1996**, *105*, 4871, and references therein.
(59) Nagle, J. F.; Tristram-Nagle, S. *Biochim. Biophys. Acta* **2000**, *1469*, 159.
(60) Gaines, F. L., Jr. *Insoluble Monolayers at Liquid−Gas Interfaces*; J. Wiley & Sons: New York, 1966.
(61) (a) Shen, Y. R. *Annu. Rev. Phys. Chem.* **1989**, *40*, 327. (b) Eisenthal, K. B. *Chem. Rev.* **1996**, *96*, 1343. (c) *Annu. Rev. Phys. Chem.* **1992**, *43*, 627. (d) Richmond, G. L. *Chem. Rev.* **2002**, *102*, 2693. (e) Richmond, G. L. *Annu. Rev. Phys. Chem.* **2001**, *52*, 357.
(62) Zhuang, X.; Miranda, P. B.; Kim, D.; Shen, Y. R. *Phys. Rev. B* **1999**, *59*, 12632.